

REFINED (**RE**presentation of **F**eatures as **I**mages with **NE**ighborhood **D**ependencies): A novel feature representation for Convolutional Neural Networks

Omid Bazgir¹, Ruibo Zhang¹, Saugato Rahman Dhruba¹, Raziur Rahman¹,
Souparno Ghosh^{2,3}, and Ranadip Pal *¹

¹Department of Electrical and Computer Engineering, Texas Tech
University University

²Department of Mathematics and Statistics, Texas Tech University

³Department of Statistics, University of Nebraska-Lincoln
ranadip.pal@ttu.edu

Abstract

Deep learning with Convolutional Neural Networks has shown great promise in various areas of image-based classification and enhancement but is often unsuitable for predictive modeling involving non-image based features or features without spatial correlations. We present a novel approach for representation of high dimensional feature vector in a compact image form, termed REFINED (**RE**presentation of **F**eatures as **I**mages with **NE**ighborhood **D**ependencies), that is conducive for convolutional neural network based deep learning. We consider the correlations between features to generate a compact representation of the features in the form of a two-dimensional image using minimization of pairwise distances similar to multi-dimensional scaling. We hypothesize that this approach enables embedded feature selection and integrated with Convolutional Neural Network based Deep Learning can produce more accurate predictions as compared to Artificial Neural Networks, Random Forests and Support Vector Regression. We illustrate the superior predictive performance of the proposed representation, as compared to existing approaches, using synthetic datasets, cell line efficacy prediction based on drug chemical descriptors for NCI60 dataset and drug sensitivity prediction based on transcriptomic data and chemical descriptors using GDSC dataset. Results illustrated on both synthetic and biological datasets shows the higher prediction accuracy of the proposed framework as compared to existing methodologies while maintaining desirable properties in terms of bias and feature extraction.

Index terms— Deep Learning, Convolutional Neural Network, Compact Feature Representation, Regression, Drug Sensitivity Prediction.

1 Introduction

In recent years, machine learning has been able to produce numerous insights from the surge of data generated in diverse areas. For instance, the area of computational biology has

benefitted from the availability of high throughput information for genome, transcriptome, proteome and metabolome. These large datasets often have the issue of numerous features with limited samples which necessitates the use of feature selection or feature extraction prior to modeling. A predictive modeling framework that has high accuracy and incorporates inbuilt feature extraction or selection can be highly useful in such circumstances. In pharmacogenomics studies, in order to predict drug efficacy, based on genomic characterizations, various types of machine learning approaches such as Random Forests, Elastic Net, Kernelized Bayesian Multi Task learning, Support vector Regression have been proposed [1, 2, 3, 4] where an initial step of feature selection or extraction has been included before model building. Although, sparse linear regression approaches such as Lasso and Elastic Net do offer embedded feature selection but the accuracy of the models are significantly lower than ensemble, kernel and non-linear regression approaches under model misspecification [1]. On the other hand, deep convolutional neural networks (CNN) has the potential to provide high accuracy prediction while automatically discovering multiple levels of joint representation of the data and thus eliminating the need for feature engineering or selection [5]. CNN bypasses the *a priori* manual extraction of features by learning them from data [6]. Furthermore, their representational richness often allows capturing of nonlinear dependencies at multiple scales [7], and minimizing generalization error rather than the training error [8].

CNN based Deep Learning methods have shown improved performance in speech recognition, object recognition [9], natural language processing [10], genomics [11] and cancer therapy [12]. Deep (multi-layered) neural networks are especially well-suited for learning representations of data that are hierarchical in nature, such as images or videos [15]. CNN-based methods have achieved close to human-level performance in object classification, where a CNN learns to classify the object contained in an image [16]. In the computational biology area, Alipanahi et al [11] used 1-D CNN architecture to predict specificities of DNA and RNA binding proteins by directly training on the raw DNA sequence. Note that 1-D CNN can be directly applied to scenarios where the features have relationships with neighbors such as DNA or RNA sequences. However, a 1-D CNN will not be highly effective in scenarios where ordering of features does not describe the dependencies among features. For instance, gene expressions or chemical descriptors, in their raw form, do not exhibit any form of ordering and hence not amenable to 1-D CNN.

If, on the other hand, the predictors are in form of images, a CNN model is often effective because the spatial correlation among the neighbors can be exploited to reduce the number of model parameters compared to fully connected network by applying convolutional operations and sharing parameters. In classification setup, [12] demonstrated the efficiency of this approach to distinguish the most prevalent subtype of lung tumor from normal lung tissue using whole slide images of The Cancer Genome Atlas (TCGA) dataset and validating on independent histopathology images. Thus, the ability to represent a collection of potentially high dimensional scalar features as images, with correlated neighborhoods, has the potential of benefiting from the automated feature extraction and high accuracy predictions of CNN based Deep Learning. To our knowledge, the only other approach for representing data as images is OmicsMapNet [13] that has been proposed at the same time while we were developing our REFINED idea. OmicsMapNet uses treemap [14] to rearrange omics data into 2D images which requires preliminarily knowledge extracted from KEGG. OmicsMapNet cannot be used when there is no ontology knowledge on the omics data, or when the covariates are non-omics data such as drug descriptors.

In this paper, we present a novel methodology, termed REFINED (**RE**presentation of **F**eatures as **I**mages with **NE**ighborhood **D**ependencies), for representing high dimensional feature vectors as mathematically justifiable 2D Images that can be processed by standard

convolutional neural network based deep learning methodologies. We illustrate the advantages of our proposed framework in terms of accuracy and bias characteristics on both synthetic and biological datasets.

2 Materials and Methods

In this section we introduce our proposed REFINED algorithm that maps high-dimensional feature vectors to images, describe the datasets used for performance evaluation, followed by the CNN architecture used as the predictive model.

2.1 REpresentation of Features as Images using NEighborhood Dependencies (REFINED)

As mentioned earlier, the main idea of the REFINED CNN approach is to map high-dimensional vectors to mathematically justifiable images for training by traditional CNN architecture. Evidently, a mapping of features from the high dimensional vector to a 2-D image matrix serially in a row by row or column by column fashion will not guarantee any spatial correlations in the image. Instead, we first obtain the euclidean distance matrix of the features and use it as a similarity measure to generate a compact 2D feature representation where neighborhood features are closely related. A potential solution to achieve this 2-D projection is to apply dimensionality reduction approach such as Multidimensional Scaling (MDS) [20] on a distance measure such as euclidean distance of features. However, that will not guarantee that each mapped point will have a unique voxel representation in the image and might result in sparse images due to the overlap [21]. For instance, if we have 900 features, the features can potentially be represented by a 30×30 matrix and a direct MDS like approach on a 30×30 dimension space might not spread out each feature in such a manner that each voxel contains only one feature. To ensure that the features are spaced out in a discrete grid and to incorporate the discrete nature of the image voxels, we apply a Bayesian version of metric MDS. We start with the MDS algorithm to create an *initial feature map* (a 2-D space with feature coordinates) that preserves the feature distances in the 2-D space with minor computational cost. Next, we apply the *Bayesian MDS* (BMDS) to estimate the feature location on a bounded domain with the constraint that each voxel can at most contain one feature. However, the location of the features are estimated up to an automorphism. Therefore, we apply a hill climbing algorithm, with a cost function that measures the absolute difference in the Euclidean distances among the new feature locations (as represented by the 2D image map) to the estimated true distances ($\hat{\delta}$, anticipating the following section) among the features, to arrive at an *optimal* configuration. More specifically, starting from the BMDS location estimates, we considered all the configurations in the map sequentially in row-order. For each feature, we tried different permutations of the features by interchanging the position of the central feature position with its neighboring features and selected the permutation that minimizes the above mentioned cost function.

The general idea of the REFINED CNN approach is shown pictorially in Figure 1 for the application case of predicting drug efficacy over a cell line using chemical descriptors of the drug as predictors.¹ In Figure 1, an example case is shown where *F-12* has been interchanged with its neighboring features, and after each exchange, we have checked the similarities/correlation among distances of features from the map and estimated distance

¹Note that we use PaDEL features as chemical descriptors of each drug.

matrix of descriptors. If we can find a better exchange case in the feature map, we exchange that feature pair and arrive at a new feature map. The entire process was repeated iteratively until we reached the optimized feature map that is close to the *benchmark* distance matrix ($\hat{\delta}$) of the initial features (in this case PaDEL descriptors).

At the conclusion of this iterative algorithm, we arrive at a REFINED feature map with all features having a unique position in a bounded 2-D space and similar features are placed close by and dissimilar features are far apart. Without loss of generality, we have considered feature maps on unit square and the BMDS specification induced sparsity in the image.

Figure 2 shows some generated REFINED images for different drugs. Each image varies from another depending on the value of the PaDEL descriptors of the drug, but the descriptor coordinates are same for all the cases.

2.1.1 Theoretical Basis for REFINED

Consider the predictor matrix $\mathbf{X} = \{x_{ij}\}, i = 1, 2, \dots, n; j = 1, 2, \dots, p$ with x_{ij} being the value of the j th predictor for the i th subject. Suppose, the predictors are generated from a latent zero mean, square integrable stochastic process $\{Z(s)\}$ where the index s belongs to a compact subset of \mathbb{R}^m . Let s_j denote the original position of the j th predictor produced by $Z(s)$ and the observed data is randomly permuted version of the original data, i.e. $x_{ij} = Z_i(s_j)$.

Case 1: There is a underlying true ordering of the predictors, i.e., there exists a permutation $\{\pi(1), \dots, \pi(p)\}$ of $\{1, 2, \dots, p\}$ such that $s_{\pi(1)} < s_{\pi(2)} < \dots < s_{\pi(p)}$ is the true, but unknown, ordering of the predictors. If such ordering exists, we can take $m = 1$ and the predictors can be projected on $[0, 1]$ via unidimensional scaling (UDS). Let $\{\hat{s}_1, \dots, \hat{s}_p\}$ be the estimated locations of the p predictors on $[0, 1]$ obtained via UDS. Let $\{\psi(1), \dots, \psi(p)\}$ be the permutation of $\{1, 2, \dots, p\}$ that orders $\{\hat{s}_1, \dots, \hat{s}_p\}$. Then under some regularity conditions $\psi(j) = \pi(j), 1 \leq j \leq p, \forall p$. Thus UDS can correctly identify the true relative pairwise distances among the predictors.

For proof, see [31].

Case 2: Suppose the ordering does not exist. For example, suppose the predictors, $x_j, x_{j'}$ and $x_{j''}$ are equidistant from one another. Clearly, $m = 1$ may not be a valid assumption and results corresponding to Case 1 become untenable in this situation. For the second order approximation, we start with $m = 2$, i.e., we would like to obtain the location of the predictors in a compact subset of \mathbb{R}^2 . Without loss of generality, we project the locations on unit square ($[0, 1]^2$).

Let d_{jk} be the observed distance between the j th and the k th predictor and δ_{jk} be their true, but unobserved, distances. Under the assumption of Euclidean metric, $\delta_{jk} = \sqrt{\sum_l (s_{j,l} - s_{k,l})^2}$, where s is now 2D coordinate system denoting the true location of the predictors j and k in unit square. As in Case 1, we can assume that $\pi(\cdot)$ is the underlying true permutation of 2D configurations of the p predictors. Our goal is to draw inference on the locations of each predictor, i.e. estimate s_j .

[32] developed a Bayesian estimation procedure to estimate $x(\cdot)$ based on observed distance by assuming $d_{jk} \sim N(\delta_{jk}, \sigma^2)I(d_{jk} > 0)$ at the data level. For the location process, we specify a spatial Homogeneous Poisson Process (HPP) with rate parameter p on unit square, i.e. $\mathbf{s} = \{s_1, s_2, \dots, s_p\} \sim HPP(p)$. Since Poisson process allows at most one event at one location, the HPP specification is essentially a constraint that allows at most one feature to occupy one voxel in the REFINED image. The model is completed by specifying diffuse Inverse Gamma priors on σ^2 . Let us denote the set of observed and true distances by \mathbf{d} and

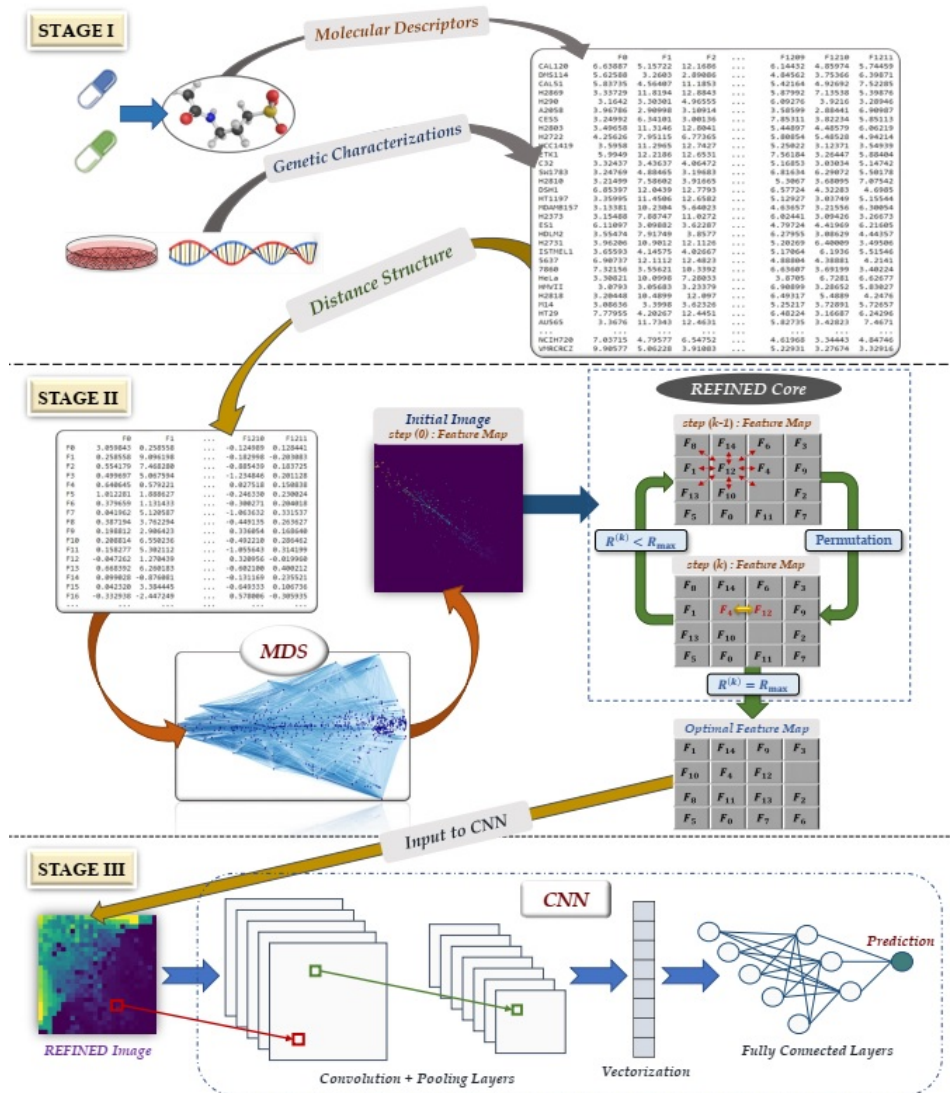


Figure 1: Overview of training a CNN using REFINED images which mainly transforms cell line-drug pairs data structures into images, (STAGE I) distance matrix of the 672 PaDEL descriptors of the cell line-drug pairs are used to calculate the distance between features, (STAGE II) Initial MDS images generated using the initial distance matrix, then hill climbing algorithm utilized as an iterative optimizer to maximize the correlation between features, by relocating the features (descriptors) in the distance matrix. (STAGE III) A CNN is trained using REFINED images and drug responses of the 60 drugs of NCI60 dataset to predict drug sensitivity of paired cell lines.

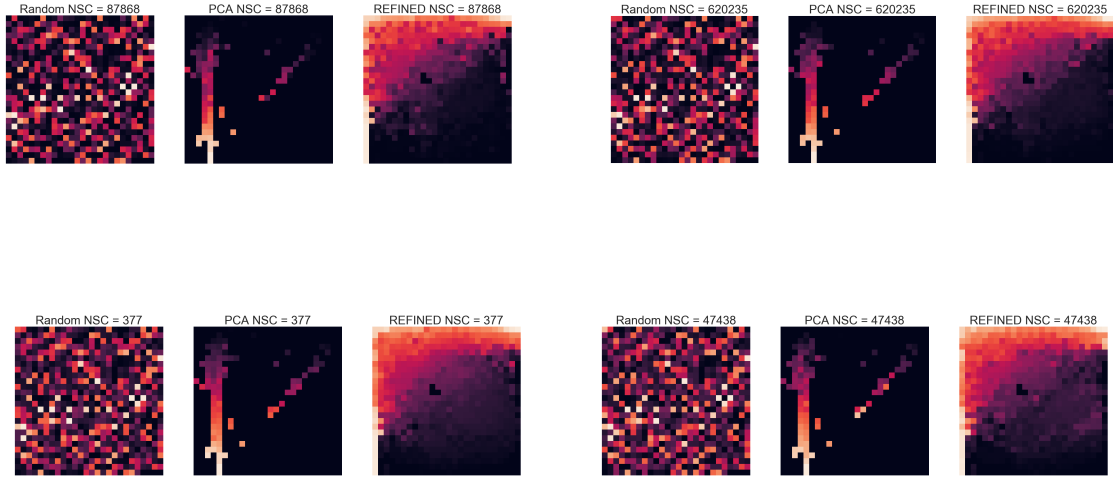


Figure 2: Illustration of generated images randomly selected from the NCI60 dataset.

$\boldsymbol{\delta}$, respectively. Our data model is then given by

$$f(\mathbf{d}|\mathbf{s}, \sigma^2) \propto (\sigma^2)^{-q/2} \exp \left[-\frac{1}{2\sigma^2} \sum_{j>k} (d_{jk} - \delta_{jk})^2 - \sum_{j>k} \log \Phi(\delta_{jk}/\sigma) \right] \quad (1)$$

where $\binom{q-p}{2}$ is the total number of distances in the dataset and $\Phi(\cdot)$ is the usual standard normal cdf. At the process level, we have

$$\mathbf{s}|p \sim \text{Uniform}(1/A(\mathbf{s})) \quad (2)$$

where $A(\cdot)$ is the area of the compact subset of \mathbb{R}^2 where the predictors are projected. Finally, the prior is given by $\sigma^2 \sim IG(a, b)$ with $a > 2$, $b > 0$ and IG denoting the Inverse Gaussian distribution. Consequently, the full posterior distribution is given by

$$[\mathbf{s}, \sigma^2|\mathbf{d}] \propto (\sigma^2)^{-q/2+a+1} \exp \left[-\frac{1}{2\sigma^2} \sum_{j>k} (d_{jk} - \delta_{jk})^2 - \sum_{j>k} \log \Phi(\delta_{jk}/\sigma) - b/\sigma^2 \right] \quad (3)$$

When q is large, $\sum \log \Phi(\cdot) \approx 0$, the full conditional posterior of $\sigma^2|.$ is approximated by $IG(q/2 + a, \frac{1}{2} \sum_{j>k} (d_{jk} - \delta_{jk})^2 + b)$. If the conditional posterior of \mathbf{s} is not available in closed form, a Metropolis-in-Gibbs sampler is used to obtain posterior realizations of the locations. Since \mathbf{s} are identifiable only up to an automorphism, convergence of the Markov Chain Monte Carlo (MCMC) is assessed on $\boldsymbol{\delta}$ and σ^2 . Furthermore, following the recommendation of [32], we used the posterior mode of \mathbf{s} as the point estimate of the covariate *location*.

Once these locations are estimated, we have a set of point-reference predictor location in the domain of interest. The domain is then subjected to regular square tessellation such that each voxel contains at most one location (as prescribed by the HPP specification). The foregoing hill climbing algorithm is then applied to arrive at the *optimal* configuration.

Once the tiled surface associated with the feature space is obtained, we have the observed value, xs_j , for each row of \mathbf{X} . The intensity at each voxel is, therefore, determined by xs_j . Voxels that do not contain any feature are assigned null values. Assuming that

the intensity at each voxel is constant, we arrive at a discrete random field- a second order approximation of the random functions developed in [31]. We can then deploy any suitable smoothing operation (for example, autoregressive spatial smoothing [33]) to generate the corresponding predictor *images* (such as shown in figure 2). Furthermore, each posterior realization of \mathbf{s} can be used for data augmentation purpose in CNN architecture. Also, since Euclidean metric is invariant under translation, rotation and reflection about the origin, any such perturbation will not affect the relationship between the response and predictors.

Note that, even if there exists ordering among the covariates, we can still generate these images in the following way. Since [31] guarantees that the relative pairwise distances among the predictors, estimated from UDS, are consistent estimators of the true relative distances, we can posit a calibration model for these estimates \hat{d}_{jk} to connect with the true distance, i.e. $\hat{d}_{jk} \sim N(\alpha_0 + \alpha_1 \delta_{jk}, \sigma^2)I(d_{jk} > 0)$.

2.2 Datasets and Preprocessing

To evaluate our framework, we considered four datasets: (a) A synthetically generated dataset (b) *NCI 60 dataset* consisting of drug responses following application of more than 52,000 unique compounds on 60 human cancer cell lines [22] (c) *Genomics of Drug Sensitivity in Cancer (GDSC)* [24] dataset that contains responses to 222 anticancer drugs across approximately 972 cancer cell lines with known genomic information. In scenario (b), we use the chemical descriptors of drugs to predict drug responses in a specific cell line. In scenario (c), we consider two heterogeneous predictor set- (i) gene expressions for around cancer cell lines and (ii) chemical descriptors of around drugs and use both these type of predictors to predict drug responses .

(a) Synthetic dataset

We simulated a synthetic dataset with P correlated features for N samples, where for each simulation 20%, 50% and 80% of the features were spurious. The features were simulated from a stationary, isotropic covariance matrix whose (i, j) th element is given by $\gamma^{|i-j|}$. We simulated different number of samples for different choices of P . For a given P , we varied N/P ratio according to 0.5, 0.8, 1, 2, 4, 6, 10. For instance, when the number of features is 100 then, 50, 80, 100, 200, 400, 600, 1000 samples were generated using the foregoing covariance matrix. We simulated the target values by simply multiplying random weights to the features. For example, N target values with 100 features ($\mathbf{X}^{N \times 100}$), with 20% spurious features were generated using the relation $\mathbf{X}[\boldsymbol{\beta}_r, \boldsymbol{\beta}_0]^T$ where $\boldsymbol{\beta}_r^{80 \times 1}$ are non-zero random weights and $\boldsymbol{\beta}_0^{20 \times 1}$ are zeros.

(b) NCI dataset

The US National Cancer Institute (NCI) screened more than 52,000 unique chemicals on around 60 human cancer cell lines. The chemical (drug) response is reported as GI50 which is the concentration required to achieve 50% of maximal inhibition of cell proliferation [22]. All the chemicals have an associated unique NSC identifier number which is assigned to identify agents when they are submitted for clinical trials to the Cancer Therapy Evaluation Program (CTEP). We used the NSC identifiers to obtain the chemical descriptor features and then used PaDEL software [23] to extract these features for each one of the chemicals. The chemicals with more than 10 % of their descriptor values being zero or missing were discarded. The final dataset consists of 52,126 chemicals, each with 672 descriptor features and 59 cancer cell lines. To incorporate the logarithmic nature of dose ad-

ministration protocol, we calculated the negative-log concentration of GI50s (NLOGGI50). The drug response distribution for one illustrative cell lines is shown in figures 3 (a). We selected 17 cell lines with more than 10k drugs, to ensure availability of enough data points for training deep learning models.

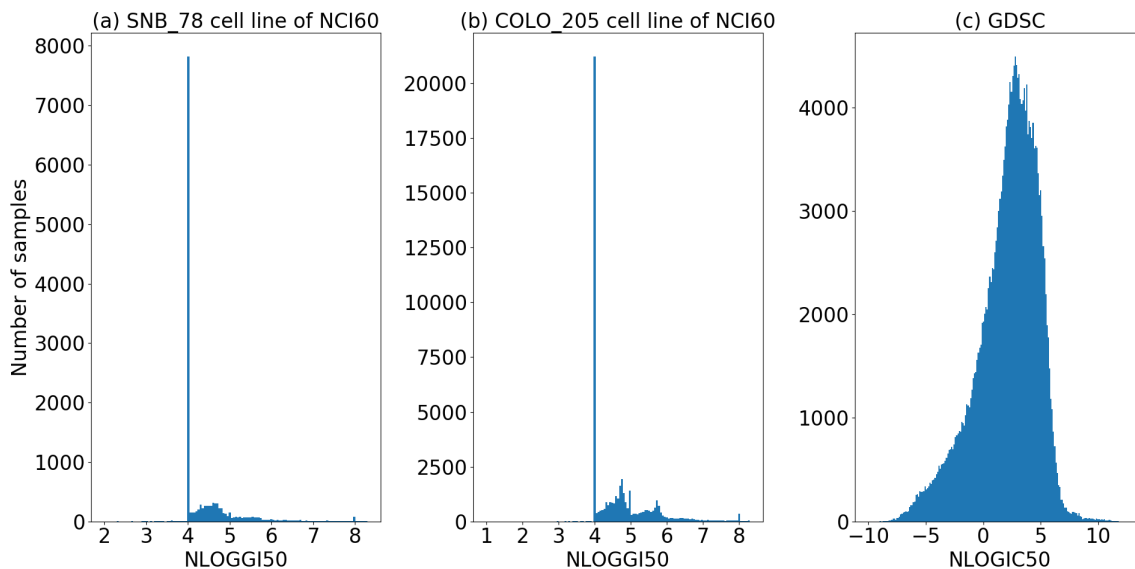


Figure 3: (a), (b) Drug response distribution of *SNB_78* and *COLO_205* cell lines of NCI60 dataset in natural logarithmic scale, where all the cell lines response distribution with more than 10,000 samples have the same large peak, (c) represents the drug response distribution in natural logarithmic scale of all the drugs that had been applied on all the cell lines available in the GDSC dataset.

(c) GDSC dataset

For validation of our framework, we also considered the Genomics of Drug Sensitivity in Cancer (GDSC) [24] dataset which describes the responses to 222 anticancer drugs across approximately 972 cancer cell lines. The resulting drug-cell line pairs have the responses reported in the form of IC50 which denotes the concentration of the drug to reduce the response by 50%. The normalized drug response distribution is shown in figure 3(b). We used the gene expression of the cell lines data (17,737 genes), and PaDel descriptors of drug data as predictors. Descriptors with more than 10 % zero or missing values were removed from the dataset, and the rest of missing values were imputed using KNN. Finally, 171K drug-cell line pairs (953 Cell lines, and 206 Drugs) are available for training.

Since in prior drug sensitivity studies [1] [2] [27], an initial feature selection was used to reduce the number of genes before training the predictive model, we also used an *a-priori* RELIEFf based feature selection [28] for scenario (c) for easier comparison with earlier studies. Since multiple drugs were tested on each cell line, a common subset of 1211 genes were selected that were found to be common among top 8000 genes selected for each drug. The gene selection process was done on the training set, then the same set of genes were used for validation and test. All the gene expressions and drug descriptors were normalized between 0 and 1.

2.3 Predictive Models

We used the REFINED images to train a CNN regressor to predict drug sensitivity of the NCI60, and GDSC datasets, as well as the simulated target values of the synthetic datasets. We compared performance of the REFINED CNN with Random Forest (RF), Support Vector Regressor (SVR), a deep Artificial Neural Network (ANN) for synthetic dataset. For other datasets, along with RF, SVR, and ANN, we compared the REFINED CNN with Elastic Net (EN), CNN with images created by randomly assigning feature coordinates (Random CNN), and CNN with images created using principal component analysis (PCA CNN) coordinates. Random CNN and PCA CNN are detailed in the section 3.1. We picked randomly 17 cell lines where more than 10k drugs were tested on them to have sufficient number of samples to train a deep learning model. Then 17 set of models were trained to predict NLOGGI50 of drugs tested on the selected cell line. In each set, all the above-mentioned models were trained on the same set of samples and tested on a separate set of same samples.

Note that for the synthetic dataset and the NCI60 dataset, the predictors are a vector of real values (chemical descriptor values for NCI60) that are converted to images. For the GDSC dataset, we have two types of input features: chemical descriptors describing the drugs and gene expression describing the cell lines. We generated individual images for each feature type and used both of them as inputs to the CNNs. For the RF, SVR, ANN, and EN these two types of features were appended and used as the predictors. We trained REFINED CNN and 6 other competing models on same set of samples, where each sample is a combination of one drug tested on one cell line. All the models were tested on a separate set of similar samples.

The distribution of NLOGGI50 shows a massive point mass at 4 (Figure 3 (a) and (b)) indicating that an overwhelming majority of drugs are not sensitive for majority of the NCI60 cell lines. Thus, we also considered a classification problem of whether a drug is sensitive or resistive among the NCI60 cell lines. Based on the NLOGGI50 distribution for different cell lines, the sensitivity threshold was empirically fixed at 4.5. All the drugs with NLOGGI50 less than the threshold (4.5) were considered resistive and the rest as sensitive. Similar to the regression scenario, we compared the CNN performance with RF, SVM, ANN, logistic regression (LR), Random CNN, and PCA CNN for the classification scenario.

2.3.1 Convolutional Neural Network

Convolutional Neural Networks (CNN) are designed to model multidimensional arrays, where convolutional layers along with pooling layer, are adaptive feature extractors connected to sequential fully connected layers [6]. A convolutional layer consists of multiple kernels connected to a local path of neurons in the previous layer, where all neurons share same parameters to generate a feature map. Thus, all neurons within the feature map scan same features in different locations of the previous layer. The pooling layer summarizes the feature map by finding the maximum/average of each adjacent kernel, which reduces the number of model parameter [5]. We used two different CNN architectures, a sequential CNN for modeling the NCI60 and synthetic dataset, and a hybrid CNN, that can accommodate drug and genetic image, for the GDSC and CCLE datasets.

The sequential CNN regressor contains seven learned layers: one input layer, two convolutional layer, three fully connected layer and one output layer. The CNN input dimension is same as the input image dimension, 26×26 . The convolutional layer contains 64, 7×7 kernels convolving with valid border mode and stride of 2, followed by batch

normalization, and ReLu activation. Each fully connected layer is followed by a batch normalization layer and ReLu activation layer. Number of neurons of the fully connected layers are respectively, 512, 256, and 64. A dropout layer with retaining probability of 0.7 was added before the output layer. While the above architecture remains same for Random CNN, PCA CNN and REFINED CNN.

The sequential CNN classifier contains input layer with the same size as the CNN regressor, three convolutional layer with 16 kernels of size 7×7 , 32 kernels of size 7×7 , and 64 kernels of size 3×3 . Each convolutional layer is followed by a batch normalization and ReLu activation layer. The third ReLu layer is followed by two fully connected layers with 256 and 64 neurons respectively. Same as the CNN regressor, each fully connected layer is followed by a batch normalization, ReLu and a drop out layer. The CNN classifier architecture remains same for Random, PCA and REFINED CNN. We used adam optimizer to train both the CNN regressor and classifier.

We used hybrid CNNs with two inputs to model GDSC dataset, where two separate images are used as inputs of the two arms of the CNN. Each arm containing two convolutional layers were concatenated, and followed by sequential fully connected layers. The two input layers represent the cell lines and drugs images, which defines each convolutional layer dimension. Each arm of CNN used to model GDSC, includes three convolutional layer with 64 kernels with size of 7×7 , stride of 1, and valid border mode, followed by batch normalization and ReLu activation function layers. Then two convolutional arms of the CNN are concatenated and connected to three sequential fully connected layers with 512,256 and 64 neurons. A bath normalization, ReLu activation function comes after each fully connected layer. A dropout layer with retaining probability of 0.7 comes before output layer. The hybrid CNN was trained by an adam optimizer. The same architecture was utilized for Random, PCA and REFINED images. There are some variation in the architecutre depending on the training set size that are explained in section 3.3.7. **All tuning parameters were chosen via nested cross validation**

2.3.2 Hyperparameter search

To tune the competitive models we did grid search on the following hyper parameters for each model using nested cross validation:

- RF: Number of decision trees in the forest and number of features evaluated at each node.
- SVM: Gamma parameter of the radial basis function (RBF) kernel.
- EN and LR: Alpha penalty term and **L1** ratio.
- ANN: Number of hidden layers (3-6), and learning rate of adam optimizer.
- CNN: As we did not have access to GPUs, we did not do comprehensive hyperparameter grid search for the CNNs. The current parameters were chosen over about hundreds of run.

3 Results

In this section, we report the performance of our REFINED-CNN methodology on the previously described synthetic, NCI60, and GDSC datasets. In each case, the performance

of the REFINED CNN was compared to ANN, RF and SVR models. We also compared the REFINED CNN with EN, Random CNN, and PCA CNN for biological datasets.

Evaluation Metric: We evaluated the performance of each regression model using (a) normalized root mean square error (NRMSE), (b) Pearsonian correlation (PCC) between the predicted and target values and (c) bias reduction. The NRMSE (4) is the ratio of the root mean squared error (RMSE) of a given model to the RMSE with mean as the predictor. It represents the overall potential of the model to minimize prediction error.

$$NRMSE = \sqrt{\frac{\sum_{i=1}^N (y_i - \hat{y}_i)^2}{\sum_{i=1}^N (y_i - \bar{y})^2}} \quad (4)$$

where the y , \bar{y} , and \hat{y} are respectively the target data, mean of the target values, and predicted target values. We offer NRMSE in order to implicitly compare all the models with respect to the baseline intercept-only model.

PCC indicates collinearity between the predicted and observed responses. Lack of collinearity often implies model misspecification and lack of predictive capability.

To represent the bias, we first generated the scatter plot of the residual (ordinate) and the observed response (abscissa). We captured the bias via the angle (θ) between the best fitted line through the residuals and the abscissa. An unbiased model is expected to produce an angle of 0° . Therefore, a smaller value of θ indicates that the model is less biased.

We used a standard t-test to report statistical significance in performance across methods. The null hypothesis is if the mean of observed value and predicted values are equal (if the predictive model detected significant portion of the observed values). Therefore, for each model we can test if:

$$H_o : \mu_{observation} = \mu_{prediction} \quad (5)$$

Then the t-test returns a p-value that expresses the probability that this null hypothesis is wrong. Hence, we used t-test to compare the predicted distribution with the observed distribution.

The classification models that predict the sensitive and resistive drugs applied on the NCI60 data cell lines, was evaluated using accuracy, precision, recall, F1 score, and area under the receiver operating characteristic curve (AUROC) metrics. Accuracy is the ratio between correct predictions; true positive (TP) and true negative (TN), over all the predictions; summation of TP, TN, false positive (FP), and false negative (FN).

$$Accuracy = \frac{TP + TN}{TP + TN + FP + FN} \quad (6)$$

Precision is the ability of predicting positive instances of the classifiers, or in other words, the ratio of correctly predicted positive instances.

$$Precision = \frac{TP}{TP + FP} \quad (7)$$

Recall or true positive rate (TPR) is the ability of the classifiers in predicting positive instances, which corresponds to the proportion of of positive instances that are correctly predicted as positive.

$$Recall = \frac{TP}{TP + FN} \quad (8)$$

F1 score is simply harmonics mean of the precision and recall,

$$F1score = \frac{2TP}{2TP + FP + FN} \quad (9)$$

False positive rate (FPR) is a ratio between negative instances that are mistakenly predicted as positive instances. AUROC combines TPR and FPR in many different threshold for each classifier on a single curve, where the area under the curve is considered as AUROC.

$$FPR = \frac{FP}{FP + TN} \quad (10)$$

3.1 Comparison with other image generation methods

In this section we consider two image generation methods, random-based and PCA-based, to compare with REFINED. In the random method, we assume each image is a matrix and the location of each entry in the vector is randomly mapped to a location in the matrix. Therefore, we placed each element of the drug descriptors or the gene expression on the image’s (matrix) coordinates one after another.

Principal component analysis (PCA) [26] is mainly used for dimensionality reduction and visualization purposes, where each sample could be represented on a 2D plane aligned with their principal eigen vectors. On the other way around, if a given matrix of a dataset is transposed, then each feature could be represented by a unique coordinate on a 2D plane. Hence, we transposed the covariates matrix where the rows are features and columns are the samples. Then the first two principal components of the transposed covariates matrix, were selected as the feature’s coordinates. Then each feature was mapped on its corresponding coordinates. Some of the generated images using the random and PCA method is shown in figure 2.

3.2 Synthetic Data

In this section, we offer the comparative performance of the candidate models on the simulated dataset. First we generate a covariance matrix for P number of features that are highly correlated along side of the diagonal and less correlated towards the off diagonal of the covariance matrix. Then the covariance matrix is utilized to generate N number of samples using the normal distribution. In each case a subset of features were randomly selected as spurious. Then random weights generated for non-spurious feature were used to generate the target values. The generated target values were normalized between 0-1. We have used REFINED to generate images for different N/P scenarios and then trained a CNN for each scenario. In each case, the same dataset was used to train RF, SVR and ANN for comparison. We used five-fold cross validation for all the models on fixed training, validation and test sets. The results are summarized in figure 4, as heat maps. As shown in figure 4, the green regions represents the cases where the REFINED-CNN NRMSE is less than the competing models. The heat maps clearly shows, that the REFINED-CNN methodology outperforms others when the number of features are relatively high (> 100) regardless of the percentage of spurious features present in the dataset. We also observe that the performance of the posited methodology improves as the N/P ratio increases. [31] also reported that the performance of their UDS based projection improved with increase in both N and P . Therefore, our findings suggest that our second order REFINED approximation are in agreement with the first order *stringing* approximation of [31]. Furthermore, we also observe that as the ratio of spurious features increases, the predictive performance of our REFINED-CNN also improves as compared to the competing models. Recall, we are not performing any feature selection for REFINED-CNN for the synthetic data. This exercise

demonstrates the ability of our approach to automatically remove spurious features without performing an explicit feature selection *a-priori*.

We next investigated the effect of the REFINED-CNN approach on the bias characteristics of the prediction. Figure 11 shows the scatter plot of prediction versus actual responses of the four models when 80 % of the features are spurious. Clearly, the scatter plot for REFINED-CNN closely follows a straight line with unit slope indicating predictive accuracy of our approach. RF and SVR reveal their well-known tendency to underpredict higher valued observation and overpredict lower valued observations [17]. REFINED-CNN bias is also better than the bias observed for the ANN scenario. Thus, it appears that the REFINED-CNN approach can automatically improve the prediction bias which some of the other existing models are known to suffer.

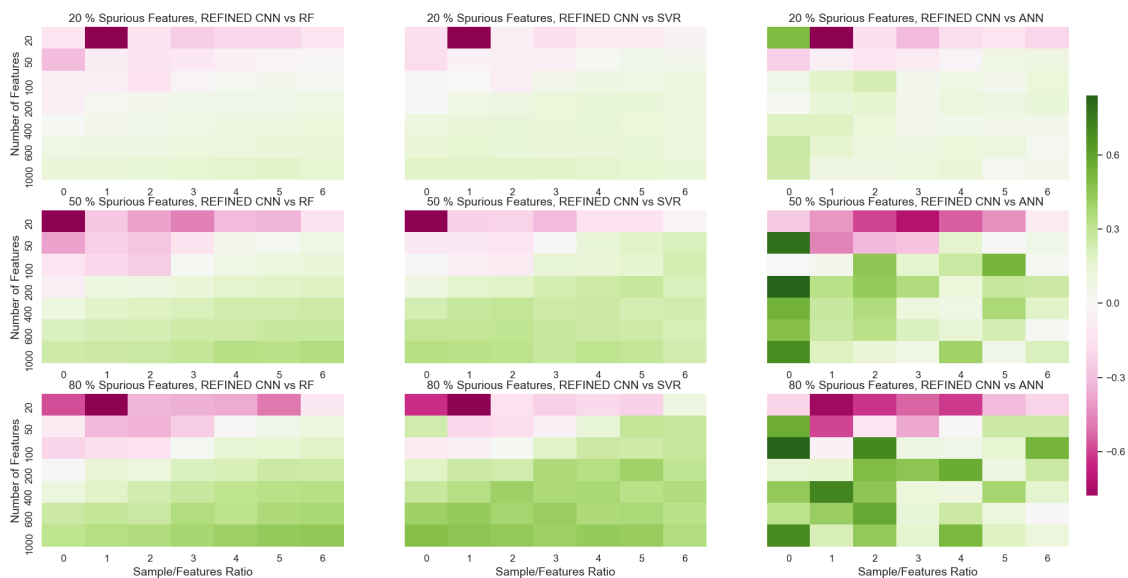


Figure 4: NRMSE difference of REFINED CNN with RF, SVR and ANN for different sample sizes and with different number of features where the 20 %, 50 % and 80 % of the features are respectively spurious. The green regions of each heatmap represents where REFINED CNN outperform other models.

3.3 NCI60 dataset

3.3.1 Classification

We investigated the discriminative power of REFINED-CNN as compared to other models in predicting resistant and non-resistant drugs on different cell lines of the NCI60 dataset. The threshold for defining resistant and non-resistant classes, was selected based on the drug response distribution shown in figure 3. The drugs with NLOGGI50 smaller than 4.25 was considered resistant and the rest as non-resistant. Since, we have sufficiently large number of drugs for each cell line ², we randomly considered 80% of the drugs for training, 10% for validation and 10% for testing. As shown in the figure 5, the REFINED CNN outperforms other classifiers for all 17 cell lines. The average classification accuracy of REFINED-CNN was 75.4% - considerably higher than the average classification accuracy obtained for Random CNN (71.6%), PCA CNN (71.7%), ANN (70.3%), RF (70%), SVM (69%) and LR(67.9%). For each model we report precision, recall, f1-score, and

²Each unique drug for a particular cell line is sample in this scenario

AUROC. REFINED-CNN outperforms other models considering all the metrics. Detailed classification results are provided in appendix tables 4, and 5. The 95 % intervals for each metric per cell lines are provided in table 7 of appendix.

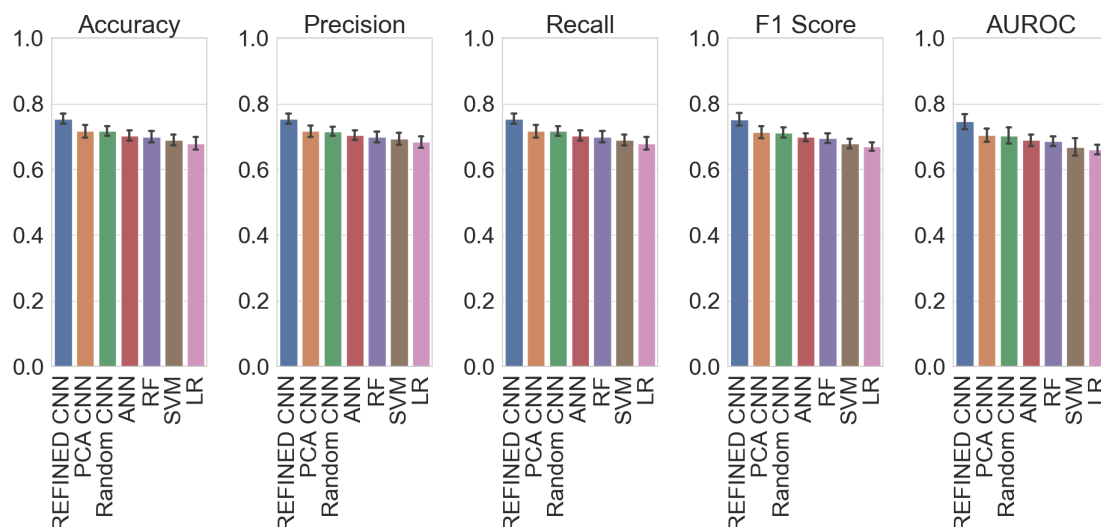


Figure 5: Summary of REFINED-CNN and 6 other competing classifier models performance on randomly selected cell lines of NCI60 database, using the accuracy, precision, recall, f1-score, and AUROC metrics.

To compare significant statistical difference between competing classifiers and REFINED CNN we used McNemar’s test that is a paired nonparametric statistical hypothesis test. McNemar’s test evaluate whether two models disagree in the same way or not. To compare classifiers with REFINED CNN classifier pairwise, a contingency table is formed and McNemar’s test is applied [37]. The null hypothesis is whether two classifiers disagree by the same amount. Therefore, if the p-value is smaller than a threshold (0.05), null hypothesis is rejected and the conclusion is: there is a significant disagreement between two classifiers. The results of comparing REFINED CNN with other models using McNemar’s test is provided in table 6.

3.3.2 Regression

The NCI60 dataset was randomly partitioned into 80% , 10% , and 10% segments for training, validation and test purpose, respectively. The same training, validation and test set were used for model comparisons. The performance of each model was evaluated using normalized root mean square error (NRMSE), Pearson correlation coefficient (PCC), bias and t-test.

Table 8 in the appendix details the performance of each model with respect to the foregoing metrics for different cell lines. The table 8 is summarized in figure 6, as bar plots. The 95 % interval for all the models per each cell line is provided in table 9 of the appendix. We note that CNN outperforms all the competing models in all 17 cell lines. The average improvement in NRMSE, PCC and bias for REFINED-CNN as compared to other competing models are 6-20%, 8-36 % , and 12-38 % , respectively .

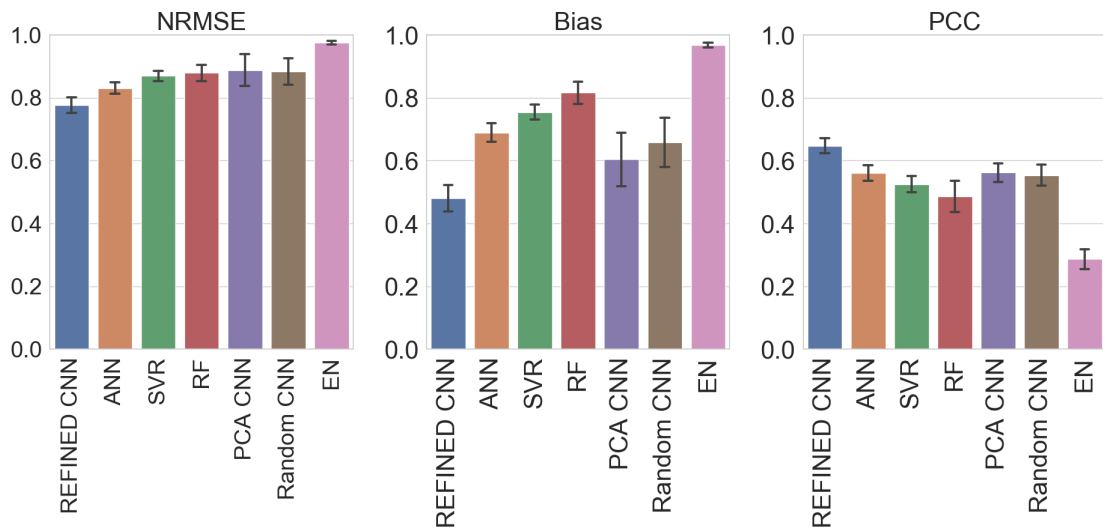


Figure 6: Summary of REFINED-CNN and 6 other competing regressors models performance on randomly selected cell lines of NCI60 database, using the NRMSE and Pearson correlation coefficients metric.

3.3.3 Data Augmentation

This section analyzes the effect of augmenting the dataset using samples from the less represented regions. As shown in figure 3(a), the massive point mass associated with the non-sensitive (resistant) drugs severely impacts a global regression model for NLOGGI50. This problem is analogous to zero-inflation problem in classical statistical literature. In such situation, the discrete point mass is modeled separately from the continuous part (see [35, 36] and references therein). In our situation, it boils down to classification into sensitive/resistive category followed by a regression in the sensitive category.

We have already demonstrated superiority of REFINED-CNN in both classification and regression in Tables 4 and 8, respectively. In this section, we explore if REFINED-CNN’s performance could be improved by synthetically oversampling the sensitive category to arrive at a more balanced dataset [34]. To that end, we used a version of SMOTE technique and generated bootstrap replicates from the sensitive category. The NRMSE improvement of REFINED-CNN regression model on different cell lines is illustrated in table 1. The bootstrap data augmentation systematically decreases the NRMSE for the cell lines indicating the negative impact of the point mass in the response distribution.

Table 1: REFINED CNN NRMSE improvement by data augmentation of the sensitive drug region using bootstrap sampling.

Cell Lines	No data augmentatoin		Bootstrap	
	NRMSE	# Samples	NRMSE	#Samples
SNB_78	0.784	13940	0.744	19613
MDA_MB_435	0.787	36868	0.762	59570
NCI_ADR_RES	0.798	37156	0.755	59250
786_0	0.752	49344	0.713	76908
COLO_205	0.741	48946	0.722	75158

Table 2: REFINED on different training size for randomly selected five cell lines

Training size	CCRF_CEM		EKVX		MDA_MB_435		NCLADR_RES		SNB_78	
	NRMSE	PCC	NRMSE	PCC	NRMSE	PCC	NRMSE	PCC	NRMSE	PCC
20 %	1.279	0.373	0.899	0.4980	0.949	0.454	0.953	0.464	0.876	0.537
40 %	0.985	0.478	0.881	0.511	0.911	0.494	0.958	0.536	0.825	0.590
60 %	0.903	0.538	0.849	0.525	0.839	0.575	0.857	0.528	0.806	0.591
80 %	0.774	0.653	0.804	0.618	0.787	0.651	0.798	0.638	0.784	0.652

3.3.4 Sample Size Analysis

Deep CNN models are expected to perform well with large number of samples and poor with small number of samples. Therefore, we trained our model on different portion of training sets for randomly selected cell lines to test this hypothesis. We trained our model on 20 %, 40 %, 60 % and 80 % of the available drugs applied on the selected cell lines and kept rest of the data for testing, considering NRMSE as comparison metric. The results of five cell lines are summarized in figure 7 which illustrates that REFINED-CNN outperforms the other models as sample size increases. This trend was also observed for the synthetic data (figure 4).

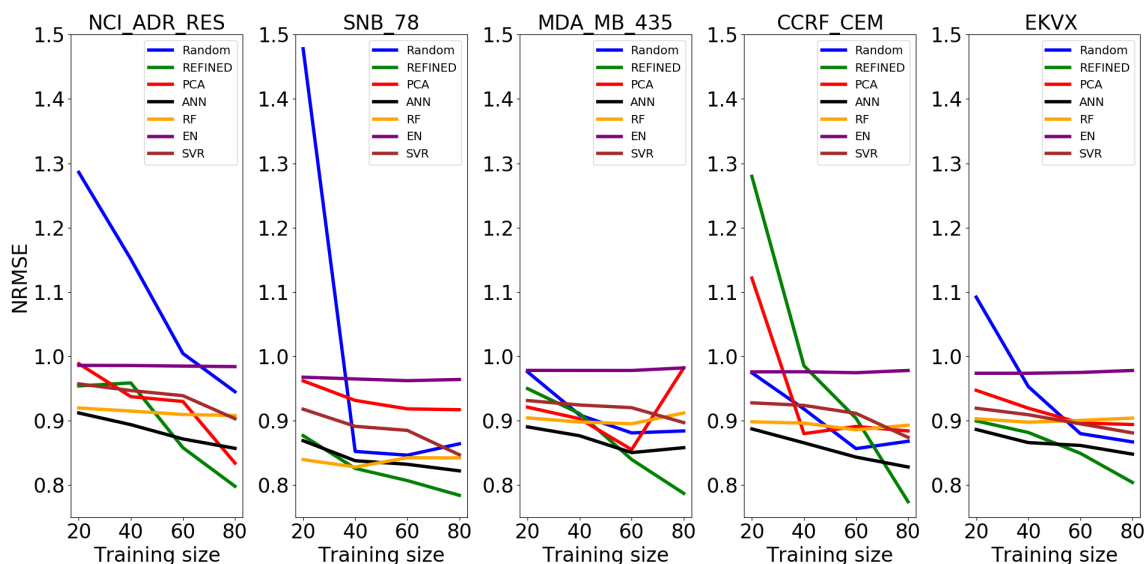


Figure 7: Comparison of six competing models with REFINED CNN on different training size of randomly selected cell line of NCI60 dataset. The x-axis represents the percentage of data used for training for each cell line. To fit the figures we shortened REFINED CNN as REFINED, Random CNN as Random, and PCA CNN as CNN in the legends.

3.3.5 Model Stacking

To explore whether stacking of multiple models can improve prediction performance, we stacked predicted drug sensitivity of the validation set of all models—in three different combinations—as the covariates in a linear regression model to find the weight of each model which are then employed to predict drug sensitivity of the test set. These three combinations are stacking non-CNN models (RF, SVR, ANN, and EN); stacking CNN models (PCA CNN, Random CNN, and REFINED CNN); and stacking all models (REFINED CNN and 6 other competitors). Figure 8 represents the stacking results where the average NRMSE of stacking all models is 0.738, stacking CNNs is 0.744 and stacking non-CNNs

0.837. By comparing the stacking results, with average NRMSE of each model in table 6, the stacking produced a significant improvement as compared to non-CNN models individually. It is notable to mention that REFINED CNN average NRMSE in table 6 is significantly lower than stacked of non-CNN models.

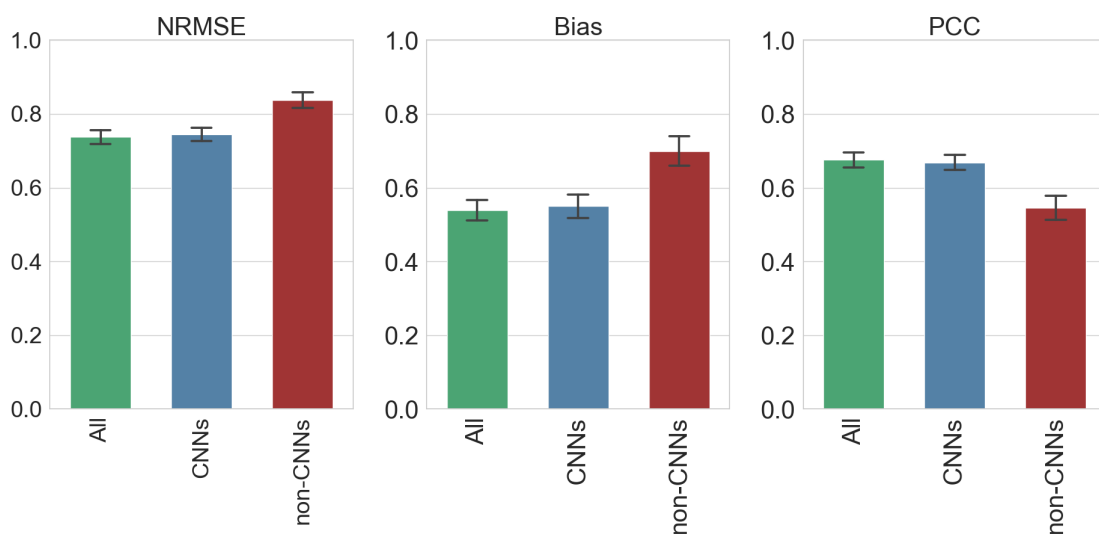


Figure 8: Comparison of stacking all models, all CNN models and non-CNN models using NRMSE, bias and Pearson correlation coefficients (PCC).

3.3.6 Bias Analysis

In this section, we re-investigate the effect of the REFINED-CNN approach on the bias characteristics of the prediction using actual biological data. Figure 9 shows the plot of the residuals against the observed values. Similar to the earlier presented synthetic data scenario, Figure 9 (a) shows that REFINED-CNN has the lowest bias (20.2°) as compared to Random-CNN (32.8°), PCA-CNN (23.8°), ANN (29.2°), RF (34.6°), SVR (33.5°) and EN (43.1°). To investigate whether bias correction erodes the advantage of REFINED-CNN in terms of bias, we considered BC1 bias correction algorithm proposed in [29] where we fit a second model (linear regression was used in this case) on the residuals. The results shown in Figure 9 (b) illustrate the superiority of REFINED-CNN in terms of lowering bias even after bias correction is applied to the competing models.

3.3.7 GDSC dataset

In this section, we consider the application of REFINED CNN that integrates two types of heterogeneous datasets. Our predictors now consist of (a) PaDel chemical descriptors representing the drugs and (b) gene expression profiles for each cell line. The response consists of the experimentally obtained IC₅₀ for each drug-cell line pair. We used the REFINED approach to generate the images corresponding to the gene expressions for each cell line and drug descriptors for each drug compound in the GDSC dataset.

Considering 222 drugs and around 800 cell lines for each drug, the total number of samples in the dataset is close to 177K. We randomly divided the dataset into 90% training, 5% validation and 5% test. Figure 10 presents the scatter plot of the natural log IC₅₀ prediction using our REFINED CNN approach, Random CNN, PCA CNN, ANN, RF, SVR, and EN along with their corresponding residual plots. Table 3 summarizes the performance

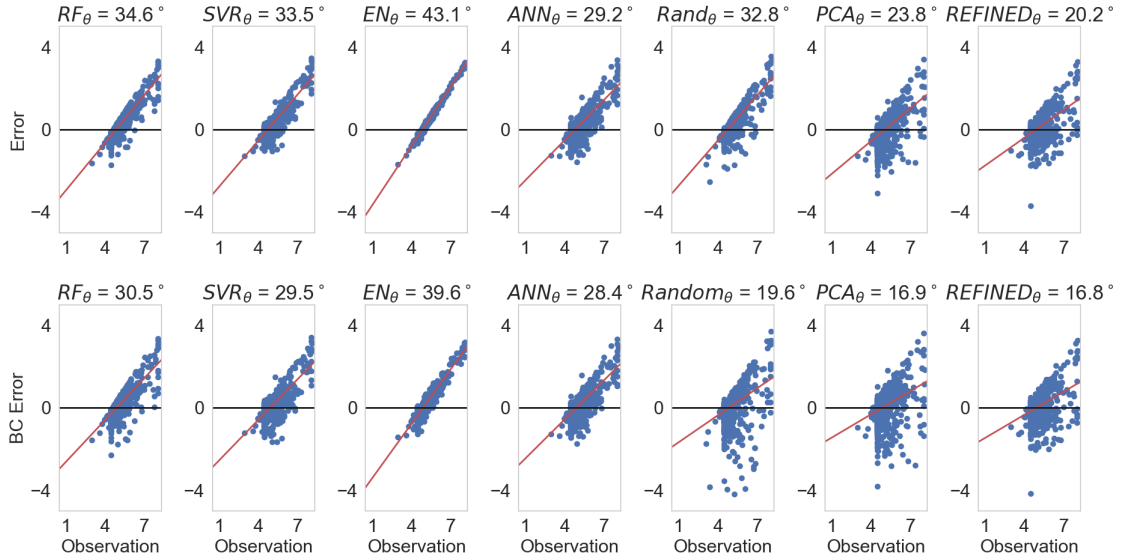


Figure 9: Residual plots for RF, SVR, EN, ANN, Random CNN, PCA CNN, and REFINED CNN for *SNB_78* cell line test set data prior bias correction (BC) (a) and post bias correction (b). The corresponding NRMSE for scenario (a) are RF = 0.842, SVR = 0.847, EN = 0.964, ANN = 0.822, Random CNN = 0.864, PCA CNN = 0.917, REFINED CNN = 0.784 and for scenario (b) are RF = 0.830, SVR = 0.836, EN = 0.937, ANN = 0.817, Random CNN = 0.832, PCA CNN = 0.840, REFINED CNN = 0.763.

of each model using NRMSE, PCC, bias, and statistical difference (p-value) metrics. We used t-test to evaluate if the predictive models detect significant portion of the observed values. Hence, large p-values can be interpreted as with high probability the predictive model doesn't capture significant portion of the observed values.

As shown in table 3, REFINED-CNN model achieves improvement as compared to other models in the range of 1-47% for NRMSE, 1-42%, for PCC. We also train the REFINED CNN on 50 % and 10 % of the GDSC data and compared it with other competing models. As the CNN architecture trained on 90 % of the REFINED images was too complex to be trained on 50 % and 10 %, we reduced the network complexity of REFINED CNN and ANN for each training size. At each step we removed one convolutional layer and one fully connected layer from the architecture explained in the section 2.3.1. The detailed corresponding results are provided in the table 10. The predicted and residual scatter plot are provided in the appendix figures 12, 13.

Table 3: Comparison of REFINED CNN, Random CNN, PCA CNN, ANN, RF, SVR, and EN performance on the GDSC dataset by measuring their NRMSE, Pearson Correlation Coefficients (PCC), and bias

Models	Trained on 10 %				Trained on 50 %				Trained on 90 %			
	NRMSE	PCC	Bias	P-value	NRMSE	PCC	Bias	P-value	NRMSE	PCC	Bias	P-value
EN	0.890	0.488	0.848	0.717	0.889	0.484	0.849	0.434	0.887	0.486	0.840	0.713
RF	0.609	0.797	0.433	0.250	0.620	0.785	0.417	0.684	0.569	0.821	0.337	0.468
SVR	0.750	0.847	0.257	0.000	0.742	0.845	0.273	0.000	0.525	0.853	0.241	0.000
ANN	1.407	0.519	0.784	0.000	0.475	0.883	0.153	0.696	0.435	0.901	0.233	0.000
Random CNN	0.579	0.836	0.215	0.000	0.456	0.892	0.193	0.000	0.424	0.906	0.166	0.000
PCA CNN	0.612	0.820	0.201	0.000	0.461	0.891	0.228	0.000	0.428	0.903	0.182	0.744
REFINED CNN	0.541	0.845	0.255	0.000	0.439	0.899	0.173	0.000	0.414	0.910	0.168	0.000

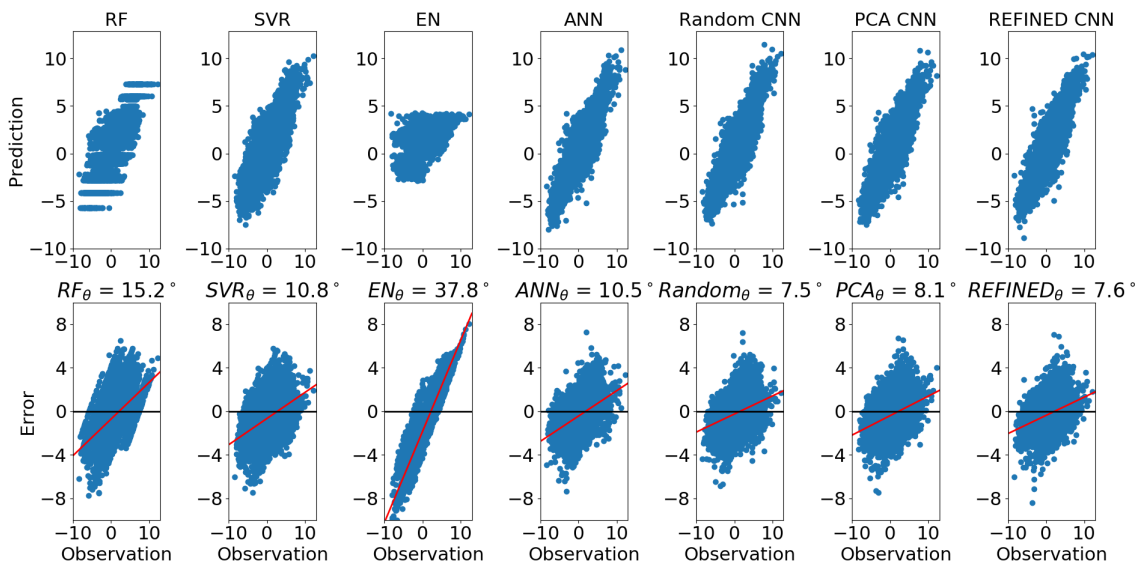


Figure 10: Scatter plot of predicted NLOGIC50s and their residual (error) for each model, in the case of models were trained on 90 % of the available data. In each scatter plot, observation is the NLOGIC50 values if the test set. On the bottom row, bias of each model is depicted by the method explained in the bias analysis section.

4 Discussion

This paper presents a novel approach of converting high dimensional vectors into images with spatial neighborhood dependency that can be used as inputs to traditional Convolutional Neural Networks. The proposed methodology was conceived from the observation that deep learning CNN has increased the prediction accuracy in many scenarios especially when the inputs are images, but it is not usually appropriate when high dimensional vectors with limited neighborhood correlations are used as inputs. Our REFINED approach produces a mapping of the input features such that spatial neighbors are close and far away points in the map are distant in initial feature space.

There are several advantages of the proposed REFINED methodology. First, the REFINED mapping to a compact image space appears to allow for *automated feature selection* using deep learning CNN architecture. Using a synthetic dataset and altering the amount of spurious features, we observed that REFINED-CNN is able to significantly outperform other approaches for scenarios with larger percentage of spurious features as shown in figure 4. Second, the REFINED CNN approach provides a *gain in predictive accuracy* as compared to three very commonly used models of Artificial Neural Networks, Random Forest, Support vector Machines, and Elastic Net. We have validated the performance of REFINED-CNN in (a) synthetic dataset, (b) NCI60 drug response dataset and (c) GDSC dataset that combines chemical descriptors of drugs with genomic expressions of cell lines. Third, REFINED-CNN methodology can also be used to seamlessly *combine heterogenous predictors* where each predictor can be mapped to an image as was done for the GDSC prediction scenario. Perhaps the biggest advantage of REFINED-CNN is that it has the potential to combine multi-type predictors, where some predictors are images, some high dimensional vectors and some having functional forms. In principle, each type of predictor data can be individually mapped to images and the corresponding images can be used as inputs in a CNN architecture. Finally, we observe that REFINED-CNN has better ability to automatically perform *bias correction* as compared to ANN, RF and SVR as shown in all three application scenarios (Figures 11, 9 and 10). The proposed REFINED approach can

also be used for data augmentation by using different realizations of the mapping as was discussed in section 2.1.1. We have provided a theoretical justification to motivate how the proposed approach can map to an ordering of features if such an ordering exists.

In terms of applications, the REFINED approach can be applied to any predictive modeling scenario where the predictors are high dimensional vectors without an explicit neighborhood based dependence structure. We motivated the application of the scenario through the drug sensitivity prediction problem where both the gene expressions and chemical descriptors are not necessarily ordered based on correlations.

Limitations of the approach will include scenarios where the covariance structure of the features is primarily diagonal with limited correlations between any features. Furthermore, the REFINED approach is expected to benefit from the traditional CNN architecture and thus the performance benefit will require large number of samples as is required for normal CNN scenarios. Also note that, REFINED is a second order approximation under Euclidean norm. If the predictor space is non-Euclidean, the current form of REFINED will not be suitable.

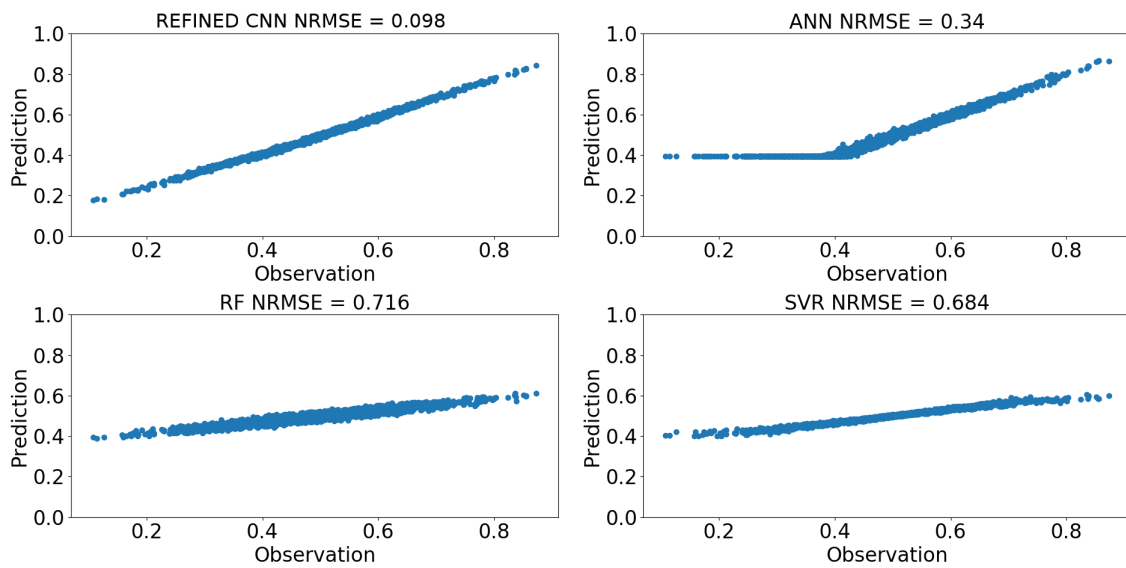
To summarize, the paper presents a novel effective tool for feature representation and multi-object regression and classification.

References

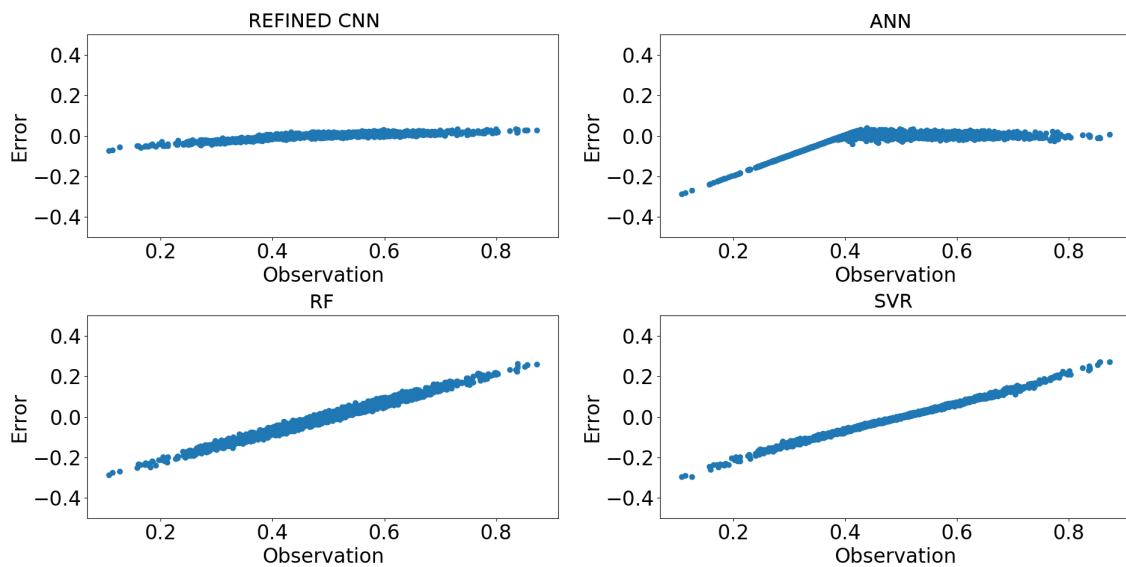
- [1] J. C. Costello and *et al.* *A community effort to assess and improve drug sensitivity prediction algorithms* Nature biotechnology, 32, (12), 1202, 2014.
- [2] Q. Wan and R. Pal. *An ensemble based top performing approach for NCI-DREAM drug sensitivity prediction challenge* PLOS One, 9, (6), e101183, 2014
- [3] Rahman, Raziur and Matlock, Kevin and Ghosh, Souparno and Pal, Ranadip. *Heterogeneity aware random forest for drug sensitivity prediction* Scientific Reports, 7, (1), 11347, 2017.
- [4] Rahman, Raziur and Otridge, John and Pal, Ranadip. *IntegratedMRF: random forest-based framework for integrating prediction from different data types* Bioinformatics, 33, (9) , 1407:1410, 2017.
- [5] LeCun, Yann and Bengio, Yoshua and Hinton, Geoffrey. *Deep learning* nature, 521 (7553), 436, 2015.
- [6] Angermueller, Christof and Pärnamaa, Tanel and Parts, Leopold and Stegle, Oliver. *Deep learning for computational biology* Molecular systems biology, 12, (7), 878, 2016.
- [7] Wainberg, Michael and Merico, Daniele and DeLong, Andrew and Frey, Brendan J. *Deep learning in biomedicine* Nature biotechnology, 36 (9) : 829, 2018.
- [8] Bengio, Yoshua. *Practical recommendations for gradient-based training of deep architectures* Neural networks: Tricks of the trade, Springer, 437:478, 2012.
- [9] Iandola, Forrest N and Han, Song and Moskewicz, Matthew W and Ashraf, Khalid and Dally, William J and Keutzer, Kurt. *Squeezenet: Alexnet-level accuracy with 50x fewer parameters and 0.5 mb model size* arXiv preprint arXiv:1602.07360, 2016.

- [10] Xu, Bowen and Ye, Deheng and Xing, Zhenchang and Xia, Xin and Chen, Guibin and Li, Shanping. *Predicting semantically linkable knowledge in developer online forums via convolutional neural network*. Proceedings of the 31st IEEE/ACM International Conference on Automated Software Engineering, 51–62, 2016.
- [11] Alipanahi, Babak and Delong, Andrew and Weirauch, Matthew T and Frey, Brendan J. *Predicting the sequence specificities of DNA-and RNA-binding proteins by deep learning* Nature biotechnology, 33 (8), 831, 2015.
- [12] Coudray, Nicolas and Moreira, Andre L and Sakellaropoulos, Theodore and Fenyo, David and Razavian, Narges and Tsirigos, Aristotelis. *Classification and mutation prediction from non-small cell lung cancer histopathology images using deep learning* Nature medicine, 24, (10), 1559, 2018.
- [13] Ma, Shiyong and Zhang, Zhen. *OmicMapNet: Transforming omics data to take advantage of Deep Convolutional Neural Network for discovery* arXiv preprint arXiv:1804.05283, 2018.
- [14] Shneiderman, Ben *Tree visualization with tree-maps: A 2-d space-filling approach* Transactions on Graphics 11 (1):92–99, 1998
- [15] Ruff, Lukas and Görnitz, Nico and Deecke, Lucas and Siddiqui, Shoaib Ahmed and Vandermeulen, Robert and Binder, Alexander and Müller, Emmanuel and Kloft, Marius. *Deep one-class classification*. International Conference on Machine Learning, 4390:4399, 2018.
- [16] Esteva, Andre and Robicquet, Alexandre and Ramsundar, Bharath and Kuleshov, Volodymyr and DePristo, Mark and Chou, Katherine and Cui, Claire and Corrado, Greg and Thrun, Sebastian and Dean, Jeff. *A guide to deep learning in healthcare* Nature medicine, 25, (1), 24, 2019.
- [17] Matlock, Kevin and De Niz, Carlos and Rahman, Raziur and Ghosh, Souparno and Pal, Ranadip. *Investigation of model stacking for drug sensitivity prediction* BMC bioinformatics, 19, (3), 71, 2018.
- [18] Chang, Yoosup and *et al.* *Cancer Drug Response Profile scan (CDRscan): A Deep Learning Model That Predicts Drug Effectiveness from Cancer Genomic Signature*. Scientific reports, 8,(1), 8857, 2018.
- [19] Chiu, Yu-Chiao and *et al.* *Predicting drug response of tumors from integrated genomic profiles by deep neural networks* BMC medical genomics, 12 , (1), 18, 2019.
- [20] Davison, Mark Leonard. *Multidimensional scaling* Wiley New York, (85), 1983.
- [21] Urpa, Lea M and Anders, Simon *Focused multidimensional scaling: interactive visualization for exploration of high-dimensional data* BMC bioinformatics, 20, (1), 221, 2019
- [22] Shoemaker, Robert H. *The NCI60 human tumour cell line anticancer drug screen* Nature Reviews Cancer, 6 (10):813,2006.
- [23] Yap, Chun Wei. *PaDEL-descriptor: An open source software to calculate molecular descriptors and fingerprints* Journal of computational chemistry, 32, (7) , 1466:1474, 2011.

- [24] Yang and *et al.*. *Genomics of Drug Sensitivity in Cancer (GDSC): a resource for therapeutic biomarker discovery in cancer cells* *Nucleic acids research*, 41, (1), 955:961, 2012.
- [25] Barretina, Jordi and Caponigro, Giordano and Stransky, Nicolas and Venkatesan, Kavitha and Margolin, Adam A and Kim, Sungjoon and Wilson, Christopher J and Lehár, Joseph and Kryukov, Gregory V and Sonkin, Dmitriy and others *The Cancer Cell Line Encyclopedia enables predictive modelling of anticancer drug sensitivity*
- [26] Wold, Svante and Esbensen, Kim and Geladi, Paul *Principal component analysis* *Chemometrics and intelligent laboratory systems*, 2, (1-3),37–52, 1987, Elsevier
- [27] Pal, Ranadip. *Predictive modeling of drug sensitivity*
- [28] Kira, Kenji and Rendell, Larry A. *The Feature Selection Problem: Traditional Methods and a New Algorithm*. Proceedings of the Tenth National Conference on Artificial Intelligence, AAAI Press, 129–134, 6, 1992.
- [29] Zhang, Guoyi and Lu, Yan. *Bias-corrected random forests in regression* *Journal of Applied Statistics*, 39, (1), 151:160, 2012.
- [30] Smouse, Peter E and Long, Jeffrey C and Sokal, Robert R. *Multiple regression and correlation extensions of the Mantel test of matrix correspondence*. *Systematic zoology*, 35, (4), 627:632, 1986.
- [31] Chen, Kun and Chen, Kehui and Müller, Hans-Georg and Wang, Jane-Ling. *Stringing high-dimensional data for functional analysis* *Journal of the American Statistical Association*, Taylor & Francis, 106, (493), 275–284, 2011.
- [32] Oh, Man-Suk and Raftery, Adrian E *Bayesian multidimensional scaling and choice of dimension* *Journal of the American Statistical Association*, Taylor & Francis, 96, (455), 1031–1044, 2001.
- [33] MacNab, Ying C and Dean, CB. *Autoregressive spatial smoothing and temporal spline smoothing for mapping rates*, *Biometrics*, Wiley Online Library, 57, (3), 949–956, 2001.
- [34] Chawla, Nitesh V and Bowyer, Kevin W and Hall, Lawrence O and Kegelmeyer, W Philip. *SMOTE: synthetic minority over-sampling technique* *Journal of Artificial Intelligence Research*, 16, 321–357, 2002.
- [35] Ghosh, Souparno and Gelfand, Alan E and Zhu, Kai and Clark, James S. *The k-ZIG: flexible modeling for zero-inflated counts*, *Biometrics*, Wiley Online Library, 68, (3), 878–885, 2012.
- [36] Ghosh, Sujit K and Mukhopadhyay, Pabak and Lu, Jye-Chyi JC. *Bayesian analysis of zero-inflated regression models* *Journal of Statistical planning and Inference*, Elsevier, 136, (4), 1360–1375, 2006.
- [37] Dietterich, Thomas G *Approximate statistical tests for comparing supervised classification learning algorithms* *Neural computation*, MIT Press, 10, (7), 1895–1923, 1998.



(a) Prediction versus observation



(b) Prediction error versus observation

Figure 11: Prediction vs observation and Error vs observation of the simulated data for REFINED CNN, ANN, RF, and SVR, where number of features, number of samples and spurious feature percentage are 1000, 10,000 and 80 % respectively. Note that the scatter plot for REFINED-CNN closely follows a straight line with unit slope indicating predictive accuracy of our approach. RF and SVR reveal their well-known tendency to underpredict higher valued observation and overpredict lower valued observations. REFINED-CNN bias is also better than the bias observed for the ANN scenario.

Table 4: Predicting sensitivity or resistivity of the drugs using seven classifiers part I, including Random CNN, REFINED CNN, and PCA CNN

Cell lines	Random CNN					REFIND CNN					PCA CNN				
	Accuracy	Precision	Recall	F1 Score	AUC	Accuracy	Precision	Recall	F1 Score	AUC	Accuracy	Precision	Recall	F1 Score	AUC
CCRF_CEM	0.725	0.723	0.725	0.723	0.716	0.752	0.751	0.752	0.75	0.743	0.721	0.72	0.721	0.717	0.708
COLO_205	0.748	0.748	0.748	0.748	0.748	0.762	0.762	0.762	0.762	0.762	0.734	0.734	0.734	0.734	0.734
DU_145	0.734	0.734	0.734	0.734	0.734	0.753	0.753	0.753	0.752	0.752	0.713	0.713	0.713	0.713	0.713
EKVX	0.713	0.713	0.713	0.713	0.712	0.747	0.748	0.747	0.747	0.747	0.709	0.709	0.709	0.708	0.707
HCC_2998	0.71	0.711	0.71	0.709	0.709	0.758	0.758	0.758	0.758	0.758	0.718	0.718	0.718	0.717	0.717
MDA_MB_435	0.713	0.712	0.713	0.706	0.692	0.757	0.757	0.757	0.754	0.742	0.692	0.696	0.692	0.693	0.69
SNB_78	0.733	0.723	0.733	0.721	0.672	0.768	0.764	0.768	0.765	0.734	0.755	0.75	0.755	0.737	0.683
NCLADR_RES	0.707	0.712	0.707	0.708	0.708	0.771	0.771	0.771	0.771	0.768	0.714	0.714	0.714	0.711	0.702
786_0	0.72	0.72	0.72	0.72	0.72	0.764	0.764	0.764	0.764	0.764	0.713	0.714	0.713	0.713	0.713
A498	0.722	0.723	0.722	0.721	0.722	0.762	0.762	0.762	0.762	0.762	0.707	0.709	0.707	0.706	0.707
A549_ATCC	0.714	0.717	0.714	0.712	0.71	0.767	0.767	0.767	0.767	0.767	0.708	0.71	0.708	0.706	0.705
ACHN	0.698	0.701	0.698	0.697	0.698	0.745	0.747	0.745	0.745	0.745	0.706	0.707	0.706	0.706	0.706
BT_549	0.719	0.718	0.719	0.716	0.711	0.747	0.749	0.747	0.745	0.739	0.7	0.701	0.7	0.7	0.699
CAKL1	0.714	0.714	0.714	0.714	0.714	0.755	0.759	0.755	0.754	0.755	0.716	0.719	0.716	0.715	0.715
DLD_1	0.722	0.717	0.722	0.695	0.642	0.779	0.775	0.779	0.775	0.745	0.734	0.728	0.734	0.716	0.666
DMS_114	0.681	0.682	0.681	0.674	0.669	0.736	0.737	0.736	0.733	0.727	0.683	0.688	0.683	0.673	0.668
DMS_273	0.705	0.701	0.705	0.698	0.679	0.704	0.704	0.704	0.691	0.669	0.762	0.76	0.762	0.76	0.747
Average	0.716	0.716	0.716	0.712	0.703	0.754	0.755	0.754	0.753	0.746	0.717	0.717	0.717	0.713	0.705

Table 5: Predicting sensitivity or resistivity of the drugs using seven classifiers part II, including LR, RF, ANN, and SVM

Cell lines	LR					RF					SVM					ANN				
	Accuracy	Precision	Recall	F1 Score	AUC	Accuracy	Precision	Recall	F1 Score	AUC	Accuracy	Precision	Recall	F1 Score	AUC	Accuracy	Precision	Recall	F1 Score	AUC
CCRF_CEM	0.666	0.672	0.666	0.647	0.638	0.695	0.695	0.695	0.689	0.678	0.685	0.693	0.685	0.67	0.66	0.698	0.697	0.698	0.692	0.682
COLO_205	0.676	0.681	0.676	0.674	0.676	0.697	0.697	0.697	0.697	0.697	0.689	0.69	0.689	0.688	0.689	0.704	0.709	0.704	0.702	0.704
DU_145	0.672	0.681	0.672	0.665	0.667	0.698	0.699	0.698	0.698	0.697	0.687	0.69	0.687	0.685	0.685	0.707	0.709	0.707	0.706	0.708
EKVX	0.655	0.658	0.655	0.655	0.657	0.669	0.669	0.669	0.669	0.669	0.659	0.659	0.659	0.659	0.659	0.672	0.673	0.672	0.671	0.67
HCC_2998	0.662	0.667	0.662	0.661	0.663	0.69	0.69	0.69	0.69	0.69	0.688	0.689	0.688	0.688	0.689	0.705	0.708	0.705	0.704	0.705
MDA_MB_435	0.682	0.687	0.682	0.664	0.65	0.699	0.698	0.699	0.691	0.677	0.694	0.699	0.694	0.678	0.663	0.706	0.705	0.706	0.7	0.687
SNB_78	0.735	0.736	0.735	0.704	0.644	0.755	0.75	0.755	0.74	0.687	0.732	0.748	0.732	0.689	0.627	0.742	0.741	0.742	0.716	0.656
NCLADR_RES	0.69	0.696	0.69	0.677	0.668	0.706	0.704	0.706	0.702	0.694	0.7	0.703	0.7	0.69	0.68	0.712	0.711	0.712	0.708	0.699
786_0	0.682	0.687	0.682	0.679	0.681	0.698	0.698	0.698	0.698	0.698	0.695	0.697	0.695	0.694	0.694	0.706	0.706	0.706	0.706	0.706
A498	0.673	0.678	0.673	0.671	0.673	0.701	0.701	0.701	0.701	0.701	0.695	0.697	0.695	0.694	0.695	0.707	0.716	0.707	0.704	0.707
A549_ATCC	0.678	0.68	0.678	0.678	0.679	0.708	0.707	0.708	0.707	0.707	0.699	0.699	0.699	0.699	0.699	0.713	0.713	0.713	0.713	0.712
ACHN	0.66	0.667	0.66	0.657	0.661	0.686	0.687	0.686	0.685	0.686	0.675	0.678	0.675	0.673	0.675	0.683	0.69	0.683	0.68	0.683
BT_549	0.673	0.687	0.673	0.656	0.654	0.702	0.705	0.702	0.697	0.691	0.692	0.705	0.692	0.678	0.674	0.7	0.711	0.7	0.689	0.684
CAKL1	0.669	0.676	0.669	0.665	0.667	0.691	0.691	0.691	0.691	0.691	0.687	0.689	0.687	0.686	0.686	0.701	0.702	0.701	0.7	0.7
DLD_1	0.713	0.707	0.713	0.682	0.628	0.71	0.698	0.71	0.695	0.647	0.706	0.704	0.706	0.666	0.612	0.719	0.709	0.719	0.702	0.653
DMS_114	0.675	0.674	0.675	0.673	0.669	0.675	0.675	0.675	0.672	0.666	0.671	0.673	0.671	0.663	0.658	0.68	0.682	0.68	0.681	0.68
DMS_273	0.687	0.685	0.687	0.671	0.649	0.712	0.711	0.712	0.701	0.679	0.672	0.681	0.672	0.638	0.619	0.704	0.7	0.704	0.698	0.68
Average	0.679	0.683	0.679	0.669	0.66	0.7	0.699	0.7	0.695	0.685	0.69	0.694	0.69	0.679	0.668	0.703	0.705	0.703	0.698	0.689

Table 6: Comparing REFINED CNN classifier with 6 other competing classifiers using McNemar’s test to discover statistical significance in predicted classes across selected cell lines.

Cell lines	RF	SVM	LR	ANN	CNN Random	CNN PCA
CCRF_CEM	0.0000	0.0000	0.0000	0.0000	0.0958	0.0007
COLO_205	0.0000	0.0000	0.0000	0.0000	0.0000	0.0254
DU_145	0.0000	0.0000	0.0022	0.0000	0.0000	0.0000
EKVX	0.0338	0.1388	0.0005	0.0000	0.0000	0.0000
HCC_2998	0.0000	0.0000	0.0020	0.0000	0.0000	0.0191
MDA_MB_435	0.0000	0.0000	0.0000	0.0162	0.0003	0.0000
SNB_78	0.0000	0.0000	0.0000	0.0000	0.0000	0.0000
NCLADR_RES	0.0000	0.0000	0.0000	0.0000	0.0000	0.0000
786_0	0.0000	0.0000	0.0359	0.2540	0.1090	0.0000
A498	0.0000	0.0019	0.7783	0.0000	0.0075	0.0000
A549_ATCC	0.0000	0.3890	0.2278	0.6717	0.0000	0.0000
ACHN	0.0000	0.0045	0.2101	0.0000	0.0000	0.0000
BT_549	0.0000	0.0000	0.0000	0.0000	0.1927	0.0000
CAKL1	0.0000	0.0000	0.0000	0.0000	0.0000	0.0000
DLD_1	0.0000	0.0000	0.0000	0.0000	0.0000	0.0000
DMS_114	0.0052	0.0024	0.9591	0.0000	0.0185	0.0000
DMS_273	0.0000	0.0000	0.0000	0.0018	0.0000	0.0000
Average	0.0023	0.0316	0.1303	0.0555	0.0249	0.0027

Table 7: Predicting sensitivity or resistivity 95 % intervals of the drugs using seven classifiers

Cell lines	Random				REFINED				PCA				LR				RF				SVM				ANN										
	Accuracy	Precision	Recall	F1 Score	AUC	Accuracy	Precision	Recall	F1 Score	AUC	Accuracy	Precision	Recall	F1 Score	AUC	Accuracy	Precision	Recall	F1 Score	AUC	Accuracy	Precision	Recall	F1 Score	AUC	Accuracy	Precision	Recall	F1 Score	AUC					
CCRF_CEM	0.018	0.031	0.018	0.018	0.019	0.017	0.017	0.017	0.017	0.018	0.019	0.019	0.019	0.019	0.019	0.021	0.020	0.021	0.021	0.021	0.020	0.020	0.020	0.020	0.020	0.020	0.020	0.020	0.020	0.020	0.019	0.019	0.019	0.019	0.019
Average	0.019	0.019	0.019	0.019	0.019	0.017	0.017	0.017	0.017	0.017	0.019	0.019	0.019	0.019	0.019	0.020	0.020	0.020	0.020	0.020	0.019	0.019	0.019	0.019	0.019	0.019	0.019	0.019	0.019	0.019	0.019	0.019	0.019	0.019	0.019

Table 8: Drug sensitivity prediction using seven regression models. The NRMSE, PCC, and bias of each model is used for comparison.

Cell lines	Random CNN			PCA CNN			REFINED CNN			RF			SVR			ANN			EN		
	NRMSE	PCC	Bias	NRMSE	PCC	Bias	NRMSE	PCC	Bias	NRMSE	PCC	Bias	NRMSE	PCC	Bias	NRMSE	PCC	Bias	NRMSE	PCC	Bias
CCRF_CEM	0.868	0.536	0.818	0.884	0.529	0.671	0.774	0.653	0.493	0.893	0.465	0.839	0.874	0.521	0.750	0.828	0.563	0.705	0.978	0.259	0.973
Average	0.884	0.554	0.659	0.888	0.562	0.605	0.776	0.647	0.481	0.880	0.486	0.816	0.870	0.525	0.755	0.831	0.561	0.689	0.976	0.287	0.968

Table 9: Drug sensitivity prediction intervals of NRMSE, PCC, and bias for seven regression models.

Cell lines	Random CNN			PCA CNN			REFINED CNN			RF			SVR			ANN			EN		
	NRMSE	PCC	Bias	NRMSE	PCC	Bias	NRMSE	PCC	Bias	NRMSE	PCC	Bias	NRMSE	PCC	Bias	NRMSE	PCC	Bias	NRMSE	PCC	Bias
CCRF_CEM	0.0029	0.0043	0.0033	0.0028	0.0043	0.0040	0.0036	0.0041	0.0043	0.0027	0.0043	0.0032	0.0029	0.0043	0.0037	0.0032	0.0043	0.0039	0.0013	0.0038	0.0014
Average	0.0027	0.0043	0.0040	0.0026	0.0043	0.0041	0.0036	0.0041	0.0043	0.0028	0.0043	0.0033	0.0029	0.0043	0.0037	0.0032	0.0043	0.0040	0.0013	0.0039	0.0015

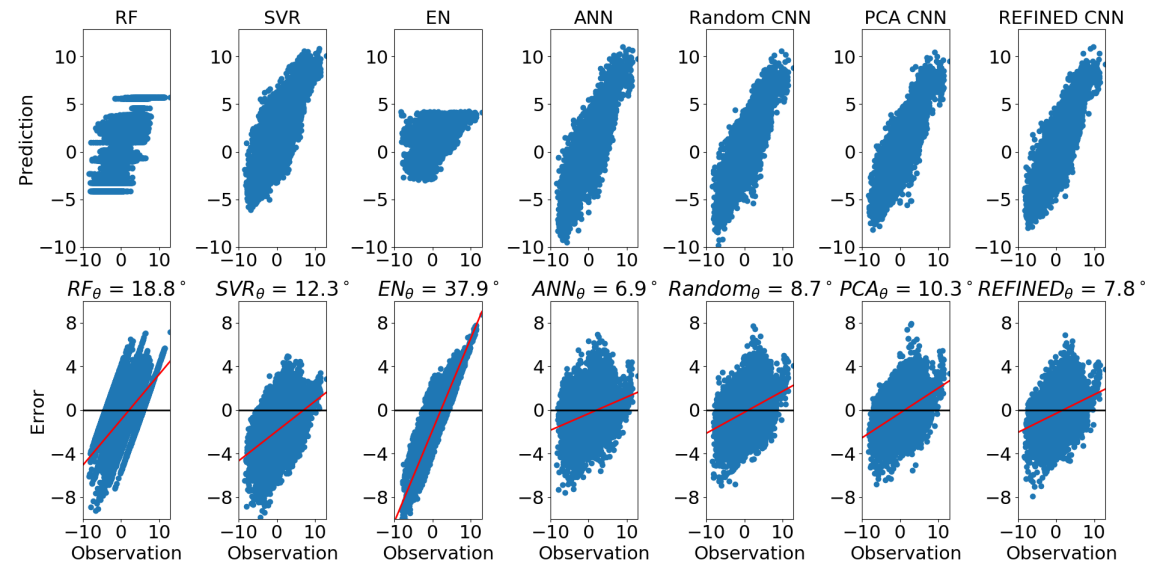


Figure 12: Scatter plot of predicted NLOGIC50s and their residual (error) for each model, in the case of models were trained on 50 % of the available data

Table 10: Statistical significance of calculated using t-test to evaluate whether the predictive model (NCI regressors) detected significant portion of the observed values distribution of NCI data.

Cell lines	Random CNN	PCA CNN	REFINED CNN	RF	SVR	ANN	EN
CCRF_CEM	0.0000	0.0000	0.0000	0.7971	0.0000	0.0049	0.8626
COLO_205	0.0000	0.0000	0.0000	0.3378	0.0000	0.4358	0.5310
DU_145	0.0000	0.1815	0.0000	0.8357	0.0000	0.7137	0.9501
EKVX	0.0000	0.0000	0.0000	0.5982	0.0000	0.9101	0.4266
HCC_2998	0.0000	0.0000	0.0000	0.3801	0.0000	0.1993	0.3928
MDA_MB_435	0.0000	0.0000	0.0000	0.8715	0.0000	0.0683	0.9771
SNB_78	0.0000	0.0932	0.0000	0.9937	0.0000	0.1175	0.9130
NCLADR_RES	0.0000	0.0000	0.0564	0.1988	0.0000	0.0006	0.3171
786_0	0.0000	0.0000	0.0000	0.1430	0.0000	0.0000	0.2506
A498	0.0000	0.0000	0.0000	0.9651	0.0000	0.0000	0.8955
A549_ATCC	0.0000	0.0116	0.0000	0.3941	0.0000	0.0098	0.5814
ACHN	0.0000	0.0188	0.0000	0.9539	0.0000	0.0000	0.9299
BT_549	0.0000	0.0000	0.0000	0.3114	0.0000	0.0117	0.1115
CAKI_1	0.0000	0.1827	0.0000	0.3207	0.0000	0.0000	0.3268
DLD_1	0.0000	0.2632	0.2490	0.7650	0.0000	0.3646	0.2584
DMS_114	0.0022	0.2367	0.0000	0.5055	0.0000	0.2343	0.5414
DMS_273	0.4277	0.0504	0.0000	0.8580	0.0000	0.8859	0.7139
Average	0.0253	0.0611	0.0180	0.6017	0.0000	0.2327	0.5870

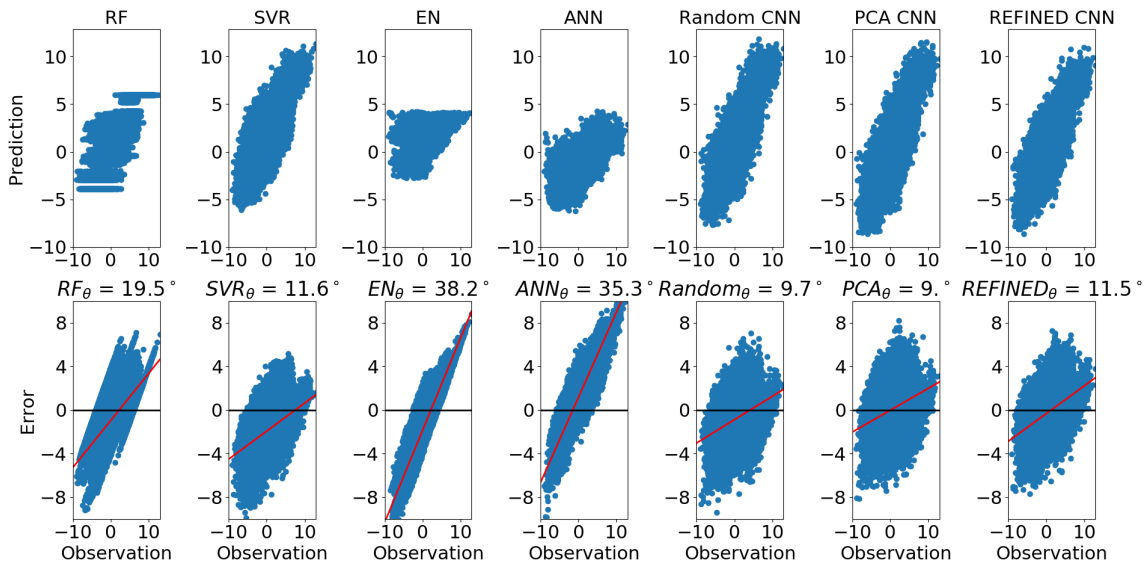


Figure 13: Scatter plot of predicted NLOGIC50s and their residual (error) for each model, in the case of models were trained on 10 % of the available data